Solar Energy Vol. 47, No. 3, pp. 237–242, 1991
Printed in the U.S.A.

0038-092X/91 $3.00 + .00

ANALYSIS OF COLLECTOR-STORAGE BUILDING WALLS USING PHASE-CHANGE MATERIALS

A. A. GHONEIM,* S. A. KLEIN,† and J. A. DUFFIE†
*Laboratory of Physics, Mathematical Eng. and Eng. Physics Dept., Faculty of Engineering, University of Alexandria, Alexandria, Egypt, †Solar Energy Laboratory, University of Wisconsin-Madison, Madison, WI 53706, U.S.A.

Abstract—The use of thermal storage walls that serve both as solar collector and thermal storage is well known. The wall is usually composed of masonry or containers filled with water to provide sensible heat storage, i.e., storage resulting from the specific heat capacity of a material as it increases in temperature. An interesting alternative to the standard materials are phase-change materials (PCMs) which employ latent heat storage. Latent heat storage utilizes the energy associated with a change of state of a material such as the transition from a solid-to-liquid, or liquid-to-gas. The solid-to-liquid phase change is preferred for many applications because of the much smaller volume change resulting in this transition for a given amount of energy storage. This paper summarizes the results of a simulation study of the use of PCMs as a collector-storage wall.

1. INTRODUCTION

The idea of using phase-change materials to replace masonry in a Trombe wall has been previously suggested by Telkes[1] and others. Experimental and theoretical tests have been done to investigate the reliability of PCMs as a Trombe wall. Bourdeau[2] tested two passive storage collector walls using calcium chloride hexahydrate. He concluded that an 8.1 cm thick PCM wall has slightly better thermal performance than 40 cm thick masonry wall. Askew[3] used a collector panel made of a thin slab of paraffin packed by a layer of insulation and mounted behind the double glazing of the building. Thermal efficiencies comparable to conventional flat-plate collectors were predicted. Collier *et al.*[4] shows that a macro-encapsulated PCM material cemented within masonry building blocks results in significant increase in the system performance over an equivalent volume of concrete.

In general, the candidate PCM must have the following characteristics to make it attractive for thermal heat storage. It must have (1) high heat of fusion, (2) high thermal conductivity to minimize thermal gradients, (3) high specific heat and density, (4) long-term reliability during repeated cycling, (5) low volume change during phase transition, (6) low vapor pressure, (7) low melting temperature, (8) be noncorrosive, nontoxic, not flammable, and (9) exhibit little or no supercooling. In this study the behavior of three phase change materials, sodium sulphate decahydrate ($NA_2 \cdot SO_4 \cdot 10\ H_2O$), medicinal paraffin, and P116-wax, are studied. The first is salt hydrate and the other two are paraffins. Salt hydrates have the advantage of low cost, high latent heat per unit weight and volume, and relatively high thermal conductivity. The main disadvantages of salt hydrates are supercooling and degradation. Paraffins have a wide range of melting temperatures, high latent heat per unit weight; they are noncorrosive, and they have negligible supercooling behavior. The main drawbacks of paraffins are low density, low thermal conductivity, flammability, and high cost[5].

The main objectives of the present study are:

1. to compare the performance of collector-storage walls using masonry and PCMs
2. to study the effect of the thermal properties of phase change materials on the performance of collector-storage walls.

The thermal properties of the materials considered in this study are listed in Table 1.

2. ANALYSIS

The one-dimensional thermal circuit network used to predict the performance of the collector storage wall is presented in Fig. 1[6]. The network uses a control function, γ, which allows ventilation of the air gap either to the building or to the environment. The wall is divided into N finite sections in the direction perpendicular to the wall. The effect of considering the energy conducted in the wall parallel to the air flow (i.e., the two-dimensional case) was studied. The energy flows in the wall parallel to the air flow were found to be approximately 0.001 of the energy conducted through the wall. For this reason, the one-dimensional model has been used to produce the following results. Figure 2 indicates the energy flows in the system. An energy balance on the collector-storage wall per unit area of the wall yields

$$q_{st} = q_s - q_l - q_b - q_v \qquad (1)$$

where

- q_s is the rate at which solar energy is absorbed on the wall surface per unit area
- q_l is the rate of energy loss through the glazing to the environment per unit area
- q_b is the rate at which energy is convected and radiated from the inside surface of the wall into the room per unit area
- q_v is the rate at which energy is carried away from the wall via airflow in the gap per unit area. Air

Table 1. Thermal properties of energy storage materials

Material	Concrete	$Na_2SO_4.10\,H_2O$	P116-Wax	Medicinal Paraffin
k_s (W/m K)	1.73	0.51	0.14	0.14
k_l (W/m K)	----	+++	+++	2.1
T_{m1}(°C)	----	32	46.7	40
T_{m2}(°C)	----	32	46.7	44
c_s (kJ/kg.K)	0.88	1.92	2.89	2.2
c_l (kJ/kg.K)	----	3.26	+++	+++
ρ_s (kg/m^3)	2286	1440	786	830
ρ_l (kg/m^3)	----	1360	+++	+++
h_{sl} (kJ/kg)	----	251	209	146

+++ assumed equal to the corresponding solid phase value

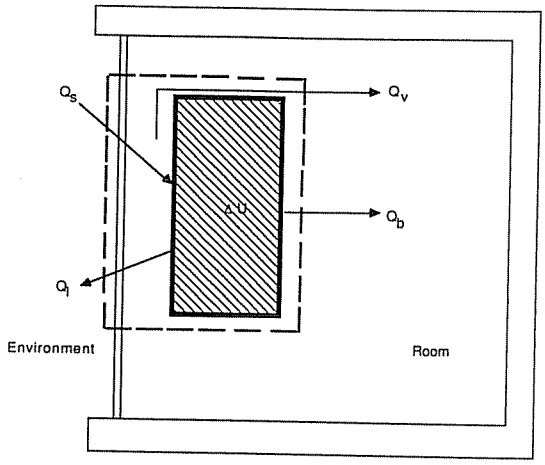

Fig. 2. Energy balance on a collector-storage wall.

circulation through the gap is assumed to be driven by density differences between the air in the gap and air in the building, i.e., thermocirculation

q_{st} is the rate of change of internal energy stored in the wall per unit area.

Integrating eqn (1) and multiplying by the collector area gives

$$\Delta U = Q_s - Q_l - Q_b - Q_v \tag{2}$$

where ΔU is the change of internal energy stored in the wall.

The terms of eqn (1) are calculated as follows:

$$\dot{q}_s = (\overline{\tau\alpha})G_s \tag{3a}$$

or

$$= G_b R_b f_i (\tau\alpha)_b + (G_d F_{c-s} + \rho G F_{c-g})(\tau\alpha)_{dr} \tag{3b}$$

$$\dot{q}_l = U_t(T_g - T_a) \tag{4}$$

$$\dot{q}_b = U_b(T_N - T_b) \tag{5}$$

$$\dot{q}_v = \frac{mc_p}{A_c}(T_o - T_i) \tag{6}$$

The terms on the right sides of eqns (3)–(6) are defined in the nomenclature. T_o, the gap outlet air temperature, can be determined from an energy balance on an incremental volume of air in the gap perpendicular to the flow[6]. The top loss heat transfer coefficient (U_t) can be calculated from a correlation developed by Klein[7], and the value of the combined radiation and convection heat transfer coefficient between the inside wall surface and the room (U_b) is assumed constant at 8.3 W/m^2 K. The analysis of PCMs can be simplified by representing the phase transition as a sensible heat process occurring over a small temperature range centered on the transition temperature. Then the rate of change of internal energy stored in the wall can be expressed as

$$q_{st} \cong \sum_{i=1}^{N} m_i \frac{dh_i}{dt} \tag{7}$$

m_i = mass of collector-storage wall node i per unit collector area; h_i = specific enthalpy of collector-storage wall node i.

The relation between the specific enthalpy and the temperature for different PCM phase conditions are as follows:

$$h(T) = c_s(T - T_{\text{ref}}) \quad \text{for} \quad T < T_{m1} \tag{8a}$$

$$h(T) = c_s(T_{m1} - T_{\text{ref}}) + \frac{h_{sl}(T - T_{m1})}{\Delta T_m} \quad \text{for} \quad T_{m1} \le T \le T_{m2} \tag{8b}$$

and

$$h(T) = c_s(T_{m1} - T_{\text{ref}}) + h_{sl} + c_l(T - T_{m2}) \quad \text{for} \quad T > T_{m2} \tag{8c}$$

where T_{m1} and T_{m2} are respectively, the lower and upper boundaries of the hypothetical transition range ($\Delta T_m = T_{m2} - T_{m1}$), T_{ref} is an arbitrary reference temperature, h_{sl} is the latent heat of the phase-change material, c_s is the specific heat in the solid range, and c_l is the specific heat in the liquid range.

By substituting eqns (3)–(8) into eqn (1), and using

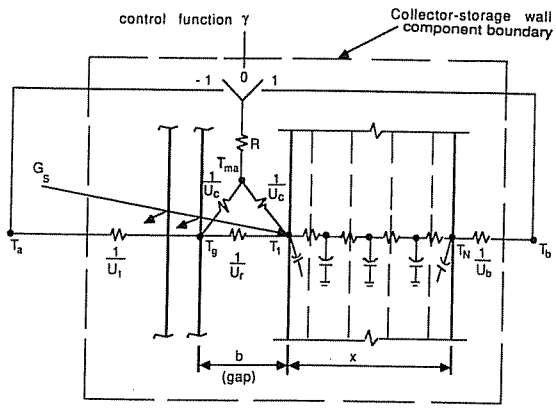

Fig. 1. Network circuit used to model collector-storage wall.

a finite difference approximation for $\frac{dh_i}{dt}$, the energy stored in the wall and the energy transformed from the wall to the building can be estimated. This model was incorporated into TRNSYS[8].

3. RESULTS AND DISCUSSION

A typical residential building with the characteristics listed in Table 2 was chosen for study.

System performance is expressed in terms of the solar savings fraction (SSF), defined by:

$$\text{SSF} = 1 - \frac{Q_{aux}}{L} \tag{11}$$

where L is the heating load (including infiltration) if the collector-storage wall were replaced by an adiabatic wall, and is given by

$$L = (UA)_{ni}(DD). \tag{12}$$

$(UA)_{ni}$ is the thermal conductance of the house when the collector storage wall is replaced by an adiabatic wall. $(UA)_{ni}$ is also termed the building load coefficient[11,12], and DD is the heating degree days[13]. (Note that solar savings fraction is not the same as the solar fraction that is commonly used in active solar heating, as the heating load L is not the total heating load in the building. The end result of interest using either solar savings fraction or solar fraction is Q_{aux}, the energy that must be purchased). The auxiliary load required by a furnace (Q_{aux}) is the heating load required when using the collector-storage wall. Energy which is transferred from the wall to the room at times when heating is not required must be dumped and does not reduce Q_{aux}.

Solar savings fraction is presented in terms of the load collector ratio (LCR), which is given by

$$\text{LCR} = (UA)_{ni}/A_c \tag{13}$$

where A_c is the collector-storage wall area.

To check the reliability of the present model, the predicted performance of a concrete storage wall was compared to the performance predicted by a solar load ratio method (SLR) developed at Los Alamos[11,12]. The two predictions agreed reasonably well. For example, the solar savings fraction values for a 0.30 m thickness of concrete for the heating season in Albuquerque at LCR = 5.55 W/m² − °K were found to be 0.65 and 0.67 using both the present model and the SLR method, respectively.

Table 2. Building characteristics[9,10]

Windows = double glazed
Ceiling heat transfer coefficient = 0.75 W/m² K
Floor heat transfer coefficient = 0.61 W/m² K
Exterior wall heat transfer coefficient = 0.55 W/m² K
Infiltration = 0.5 air change per hour
Internal gains = 555 W
Glazing (Storage Wall) = double
Vent area (Storage Wall) = 3% of total wall area

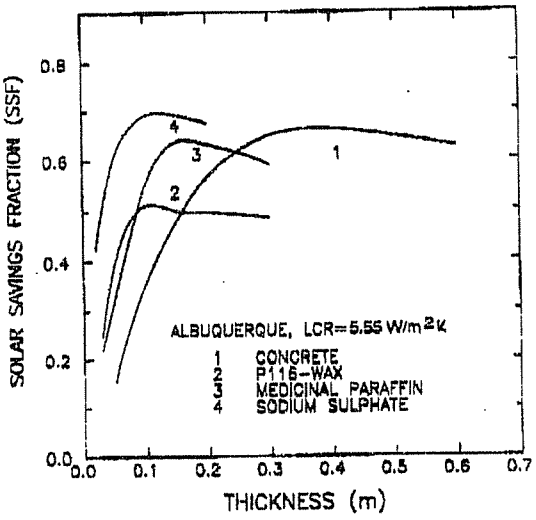

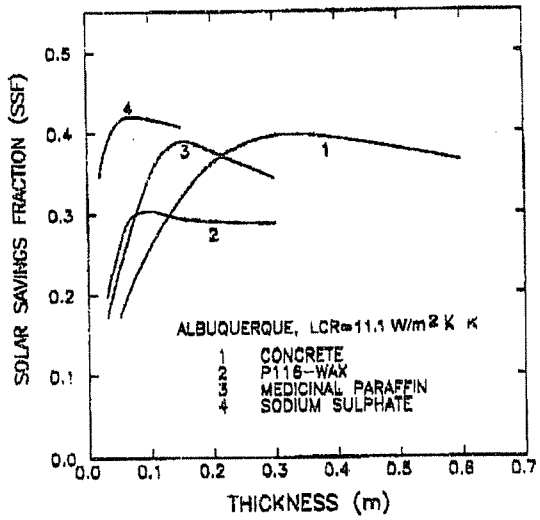

Fig. 3. (a) Variation of solar savings fraction with wall thickness for different storage media (vent area = 3% of wall area). (b) Variation of solar savings fraction with wall thickness for different storage media (vent area = 3% of wall area).

Figures 3(a) and (b) show the variation of the solar savings fraction with thickness at different values of the load collector ratio (LCR), for the three different storage media investigated in this study. These results were generated using typical meteorological year (TMY) data for Albuquerque for the heating season (from Nov. 1 to Apr. 1). All the materials show an optimum thickness which can be explained as follows. The SSF first increases with increasing wall thickness because the storage mass carries over enough solar energy to heat the building then decreases because of the increased thermal resistance of the wall. To further investigate this behavior, the effect of air vents was studied. As seen from Fig. 4, the performance of the collector-storage wall without air vents sharply decreases as thickness increases because heat conduction is the only mechanism for energy transfer from the wall to the room and the thermal resistance increases with increasing thickness.

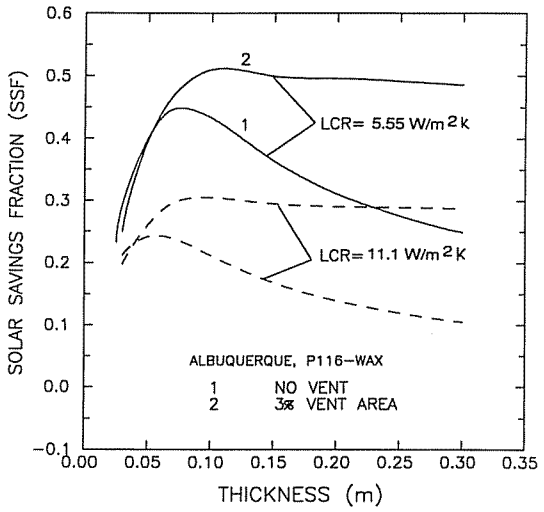

Fig. 4. A comparison of the performance of vented and unvented storage walls for P116-Wax.

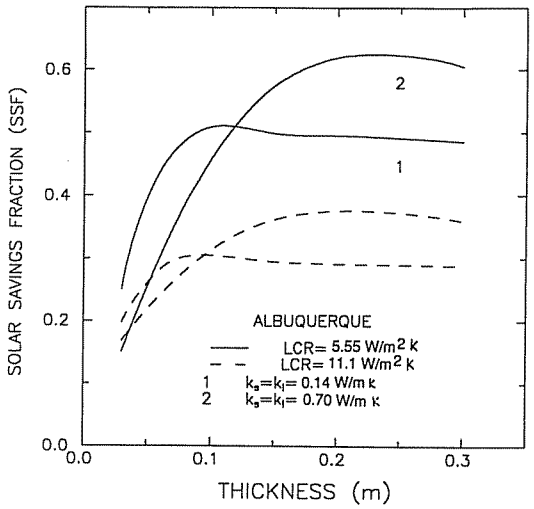

Fig. 5. Variation of solar savings fraction with wall thickness and thermal conductivity for P116-Wax (vent area = 3% of wall area).

Figures 3(a) and (b) show sodium sulphate decahydrate to have the best computed thermal performance. A wall of sodium sulphate decahydrate can achieve the same performance of concrete storage wall with a thickness approximately five times larger (without consideration for the support materials for the PCM). For paraffins, a wall with half thickness of concrete can give the same performance, i.e., approximately one sixth the storage mass. The excellent performance of sodium sulphate decahydrate can be attributed to its relatively low melting temperature (32°C) and its relatively high thermal conductivity. The main problems involved in using sodium sulphate decahydrate (Glauber's salt) are the occurrence of supercooling and stratification which were not considered in the simulations. Telkes[14] indicated that a 4% concentration of a nucleating agent like borax (sodium tetraborate decahydrate) prevents supercooling in $NA_2 \cdot SO_4 \cdot 10\ H_2O$, and reported that a marked improvement in the problem of stratification can be achieved by mixing in a thixotropic agent.

The performance of paraffins can be improved by increasing the thermal conductivity and by using paraffins with low melting temperature. Paraffins can have a wide range of melting temperatures. The thermal conductivity of paraffins can be increased by using a filler with a higher thermal conductivity. Figure 5 shows the potential improvement in the performance due to increasing thermal conductivity at different values of LCR. Figures 6–8 are generated using the optimum thickness for the P116-wax, i.e., 0.12 m (from Fig. 3(a).

Figure 6 shows the variation of SSF with melting temperature at two different thermal conductivities. At a low transition temperature (25°C), and a large thermal conductivity (0.70 W/m − °K), the solar savings fraction (SSF) has the highest value because the rate of heat conduction to the interior surface of the wall and into the room in this case causes most of the wall to reach its transition temperature. Once charged, the wall discharges and loses heat at a lower rate. The average liquid fraction over the heating season period for this case was found to be approximately equal to 0.85, and the PCM operates in the liquid phase mode most of the time. For a high phase transition temperature (46.7°C), and a larger thermal conductivity, the system performance is low because during charging, heat is conducted to the interior surface of the wall and into the room at such a rate that the wall is at its melting temperature only a small fraction of the time. Once charged, the wall discharges and loses heat to the environment. The average liquid fraction over the heating season period in the case was found to be approximately equal to 0.12, and the PCM behaves approximately as a sensible store. At a high melting temperature and low thermal conductivity, the performance is slightly improved. In this case there is a compromise between the heat conduction rate

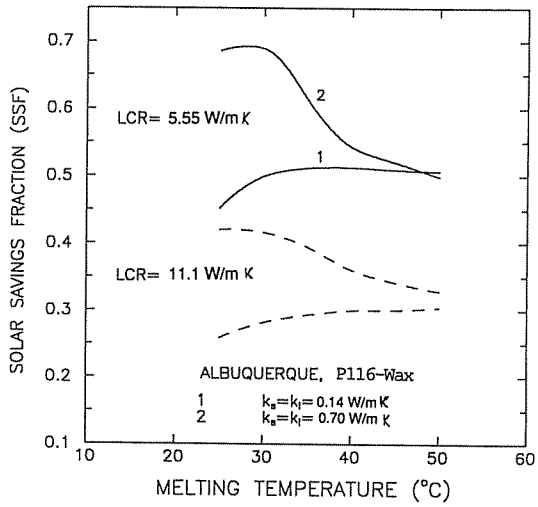

Fig. 6. Variation of solar savings fraction with melting temperature (h_{sf} = 209 kJ/kg) at different thermal conductivities (vent area = 3% of wall area).

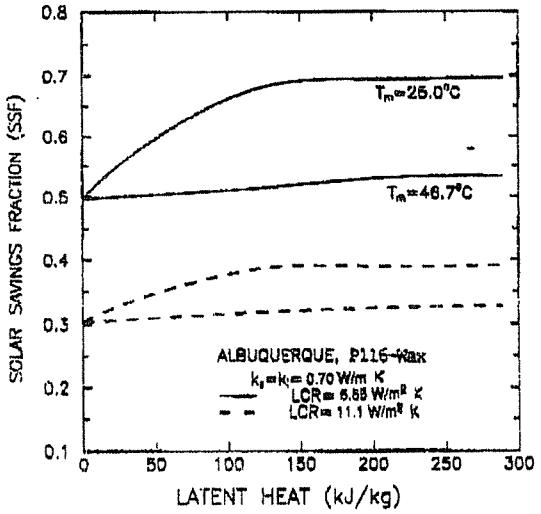

Fig. 7. Variation of solar savings fraction with latent heat at different melting temperatures and LCR (vent area = 3% of wall area).

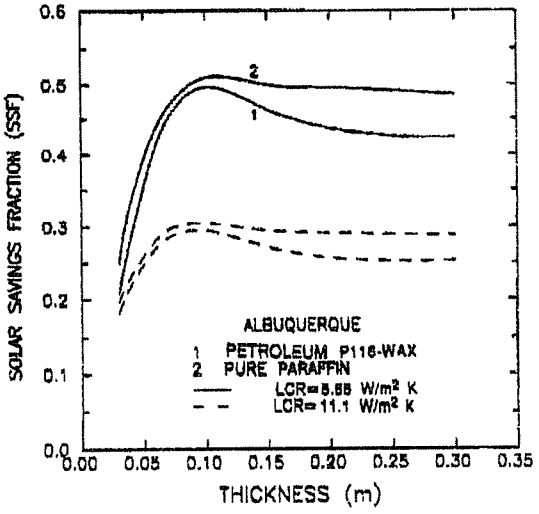

Fig. 9. Variation of solar savings fraction with thickness for industrial grade and pure paraffins (vent area = 3% of wall area).

through the wall during charging and the heat loss rate during discharging.

Figure 7 shows the variation of SSF with latent heat at different melting temperatures and with LCR. The latent heat of paraffins varies between 129–289 kJ/kg. As the latent heat increases, the amount of energy stored in the material increases and this subsequently increases the solar savings fraction. But, as seen from the figure, the latent heat has a little effect on the SSF value. For high melting temperature (46.7°C), the behavior of the PCM is approximately equal to that for the concrete wall, and no significant improvement in the system performance can be realized with PCM with such high temperatures. To confirm this behavior, the liquid fraction was calculated. The average liquid fraction over the heating season period was found to be approximately 0.14, i.e., the PCM operates most of the time in the solid phase (i.e., sensible store).

Figure 8 shows the effect of melting temperature bandwidth for industrial grade paraffins. The industrial grade paraffins were assumed to have a melting temperature bandwidth up to 20°C, i.e., ±10°C around the nominal melting temperature. As seen from the figure, the melting temperature bandwidth has little effect on the system performance. Figure 9 compares between the industrial grade paraffins (h_{sl} = 129 kJ/kg, ΔT_m = ±10°C), and pure paraffins (h_{sl} = 209 kJ/kg, ΔT_m = 0°C) at different thicknesses. Up to the optimum thickness, there is a little difference between the system performance predicted for both industrial grade paraffins and pure paraffins. The industrial grade paraffins can be used directly as a storage wall material, taking advantage of their reduced cost.

Figure 10 was generated using wax with the best thermal properties in the range investigated, i.e., T_m = 25°C, and k_s = k_l = 0.70 W/m − °K. As seen from the figure, there is a significant increase in the system performance in comparison with the performance of

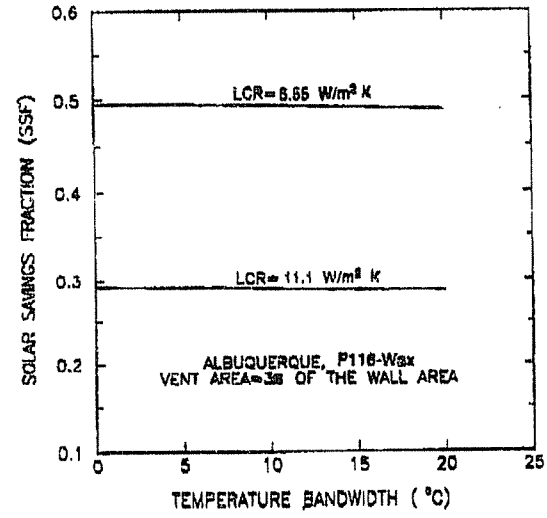

Fig. 8. Variation of solar savings fraction with melting temperature bandwidth for industrial grade paraffins (T_m = 46.7°C).

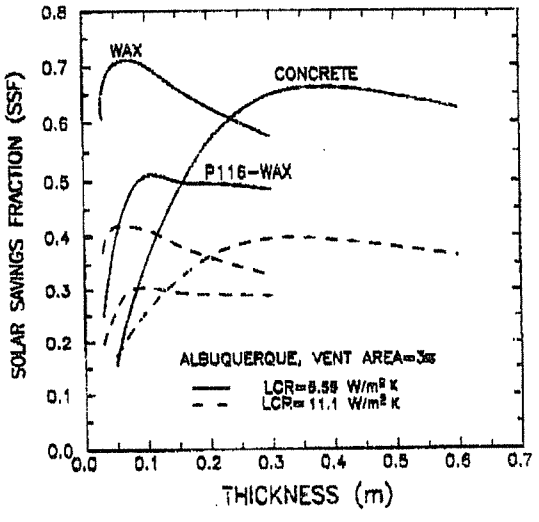

Fig. 10. Variation of solar savings fraction with thickness for concrete, P116-Wax, and Wax (k_s = k_l = 0.70 W/mk, T_m = 25°C).

both concrete and P116-wax (T_m = 46.7°C, and $k_s = k_l$ = 0.14 W/m − °K).

In conclusion, phase-change materials seem to be candidate materials for use in solar passive systems, and they may be preferable alternatives to the use of sensible store (masonry and water) as a storage wall on the basis of volume, mass, and thickness. Finally, proper attention should be given to the selection of PCMs containers. The PCM and its packaging should be chemically compatible to insure long term durability of the containers. The container must also provide an efficient heat transfer surface for energy exchange between the storage material and the building.

Acknowledgments—The financial support of the Egyptian government during this study is appreciated.

NOMENCLATURE

A_c collector-storage wall area
b spacing between wall surface and first cover glazing
c_s specific heat of PCM in solid phase
c_l specific heat of PCM in liquid phase
C_p specific heat of air
DD heating degree days
f_i fraction of the collector irradiated by direct beam
F_{c-g} collector radiation view factor of the ground
F_{c-s} collector radiation view factor of the sky
G instantaneous total solar radiation on a horizontal surface
G_b instantaneous beam solar radiation on a horizontal surface
G_d instantaneous diffuse solar radiation on a horizontal surface
G_s mean solar radiation incident on a shaded collector
h_i specific enthalpy of a collector-storage wall node i
h_{sl} latent heat (solid-liquid transition)
k_s thermal conductivity of PCM in solid phase
k_l thermal conductivity of PCM in liquid phase
L heating load (including infiltration)
m_i mass of collector-storage wall node i
m mass flow rate
q_b is the rate at which energy is convected and radiated from the inside surface of the wall into the room per unit area
q_l is the rate of energy loss through the glazing to the environment
q_s is the rate at which solar energy is absorbed on the wall surface per unit area
q_{st} is the rate of change of internal energy stored in the wall per unit area
q_v is the rate at which energy is carried away from the wall via airflow in the gap per unit area (air circulation through the gap is assumed to be driven by density differences between the air in the gap and air in the building i.e., thermocirculation).
Q_b energy transferred from the inside surface of the wall into the room
Q_l energy loss through the glazing to the environment
Q_v energy vented from collector-storage wall to the building
Q_{aux} auxiliary heating energy
R_b ratio of incident beam radiation on the collector surface to incident beam radiation on the horizontal surface
t time
T_a ambient air temperature
T_b building temperature
T_g temperature of the inside glazing of the double glazed collector-storage wall
T_i gap inlet air temperature
T_m nominal melting temperature
T_{ma} mean air temperature in the gap
T_{m1} lower boundary of the transition range
T_{m2} upper boundary of the transition range
T_N temperature of the inside surface of the collector-storage wall
T_o gap outlet air temperature
T_{ref} arbitrary reference temperature
T_1 outside surface temperature of the collector-storage wall
$(UA)_{ns}$ thermal conductance of the house if the storage-collector wall is replaced by an adiabatic wall
U_b the combined radiation and convection heat transfer coefficient between the inside wall surface and the room
U_c convection heat transfer coefficient
U_t collector-storage wall top loss coefficient
U_v equivalent radiation heat transfer coefficient
ΔU change of internal energy of the storage material.
ΔT_m transition range width
γ control function
ρ ground reflectance
ρ_s density of PCM in solid phase
ρ_l density of PCM in liquid phase
$(\overline{\tau\alpha})$ average transmittance-absorptance product
$(\tau\alpha)_b$ transmittance-absorptance product for beam radiation
$(\tau\alpha)_{dr}$ transmittance-absorptance product for diffuse and ground reflected radiation

REFERENCES

1. M. Telkes, Trombe wall with phase change storage material, *Proceedings of the 2nd National Passive Solar Conference,* Philadelphia, PA (1978).
2. L. E. Bourdeau, Study of two passive solar systems containing phase-change material for thermal storage, *Proceedings of the 5th National Passive Solar Conference* (1980).
3. G. L. Askew, Solar heating utilizing a paraffin phase-change material, *Proceedings of the 2nd National Passive Solar Conference,* Philadelphia, PA (1978).
4. R. K. Collier and D. P. Grimmer, The experimental evaluation of phase-change material building walls using small passive text boxes, *Proceedings of the 3rd National Passive Solar Conference,* San Jose, CA (January 1979).
5. D. Hale, M. Hoover, and M. O'Neill, *Phase change-materials handbook,* NASA CR-61363, NASA George C. Marshall Space Flight Center (1971).
6. D. M. Utzinger, Analysis of building components related to direct solar heating of buildings, *M.S. Thesis,* University of Wisconsin-Madison, Solar Energy Laboratory (1979).
7. S. A. Klein, Calculation of collector loss coefficients, *Solar Energy* **17** (1975).
8. S. A. Klein, *et al.* TRNSYS, A transient simulation program, University of Wisconsin-Madison, version 13.1x (1988).
9. *ASHRAE handbook of fundamentals,* New York, American Society of Heating, Refrigeration and Air-Conditioning Engineers, Inc. (1977).
10. *ASHRAE handbook of fundamentals,* New York, American Society of Heating, Refrigeration and Air-Conditioning Engineers, Inc. (1981).
11. J. Balcomb, *et al., Passive solar design handbook* (vol. 2), ASES, Boulder, CO (1980).
12. J. D. Balcomb, *et al., Passive solar design handbook* (vol. 3), ASES, Boulder, CO (1982).
13. D. G. Erbs, *et al.,* Estimation of degree-days and ambient temperature bin data from monthly-average temperatures, *ASHRAE Journal* (June 1983).
14. M. Telkes, Thermal storage for solar heating and cooling, *Proceedings of the workshop on solar energy storage subsystems for the heating and cooling of buildings,* NSF-RA-N-75-051, University of Virginia (1975).